Analysis of the Dissolution and Crystallization of Partly Immiscible Ternary Mixtures Using a Composite Sensor Array of In Situ ATR-FTIR, Laser Backscattering, and Imaging

I&EC research
Industrial & Engineering Chemistry Research

pubs.acs.org/IECR

Article

Analysis of the Dissolution and Crystallization of Partly Immiscible Ternary Mixtures Using a Composite Sensor Array of In Situ ATR-FTIR, Laser Backscattering, and Imaging

Elena Simone,* Gillian Beveridge, Pauline Sillers, Jennifer Webb, Neil George, and John Hone

Cite This: *Ind. Eng. Chem. Res.* 2022, 61, 18514−18529

Read Online

ACCESS | Metrics & More | Article Recommendations | Supporting Information

ABSTRACT: The thermodynamic phase diagram of an agrochemical active ingredient (AI) in water and acetone was determined using an array of process analytical technology (PAT) tools and equilibrium experiments. This ternary system was found to separate into multiple liquid phases at certain temperatures and concentrations (oiling out). Furthermore, agglomeration of the solid particles was observed at specific conditions. Signals from laser backscattering, attenuated total reflection infrared spectroscopy, and in situ imaging were used to study oiling out and to understand the interactions among the different phases and how they affected the dynamics of dissolution and crystallization of the AI. Characterizing partly immiscible ternary mixtures is a challenging task due to the presence of multiple dispersed phases such as droplets, particles, and agglomerates that are difficult to discriminate using traditional analytical techniques. The approach proposed here combines and integrates signals from multiple complementary online measurements to understand and monitor such complex systems.

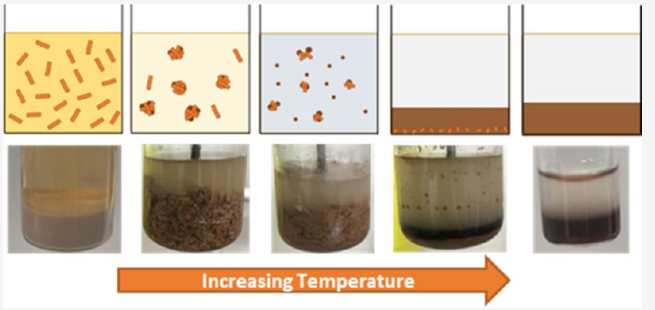

INTRODUCTION

Crystallization is a widely used separation and purification technique. The correct design and control of crystallization processes allows delivery of consistent crystal properties (e.g., size, purity, polymorph) to ensure product quality (e.g., solubility, bioavailability) for pharmaceutical, agrochemical, or food applications, to name a few.[1−3] Most crystallization studies present in the literature are carried out using model systems with high purity, with a limited amount of impurities or with deliberately added additives.[4−6] However, real industrial crystallization processes, particularly in the food and agrochemical industries, involve multiple impurities that can affect both thermodynamic and kinetic aspects of crystallization. Furthermore, economic and sustainability considerations might lead to the use of mixtures of solvents that are only partially miscible together with the crystallizing compound, giving rise to the oiling out phenomenon, also called liquid−liquid phase separation (LLPS) or liquid−liquid demixing. During oiling out, a ternary mixture comprising one liquid phase at a specific concentration of solute separates into two different liquid phases with different solute concentrations and densities.[7−11]

Oiling out is usually an undesired phenomenon as it can affect, for example, (1) the kinetics of crystal nucleation and growth, due to the different supersaturations of the solute in the two liquids; (2) the rheology of the crystallizing suspension, disturbing mixing and downstream operations (e.g., filtration), (3) the overall purification yield, as the main solute and impurities will have different solubilities in the two liquid phases. Additionally, oiling out can cause undesired fouling of surfaces and agitators.[11−13]

To predict and eventually avoid oiling out during processing, it is essential to have a good knowledge of the ternary phase diagram of the crystallizing compound in the two solvents used. Furthermore, it is important to understand how the different phases interact in different regions of the phase diagrams, particularly when solid particles are coexisting with multiple liquid phases at different compositions. In fact, such interactions will affect the crystal shape and size distributions during the crystallization process.

Oiling out phenomena do not always have negative processing consequences. In some cases, the aforementioned interactions between solid and liquid phases can be controlled during liquid−liquid phase separations to enhance the size and shape distributions of a population of crystals. In fact, with appropriate seeding in the region of liquid−liquid, it is possible to form agglomerates. This can be especially useful for needle-

Received: September 27, 2022
Revised: November 22, 2022
Accepted: November 24, 2022
Published: December 7, 2022

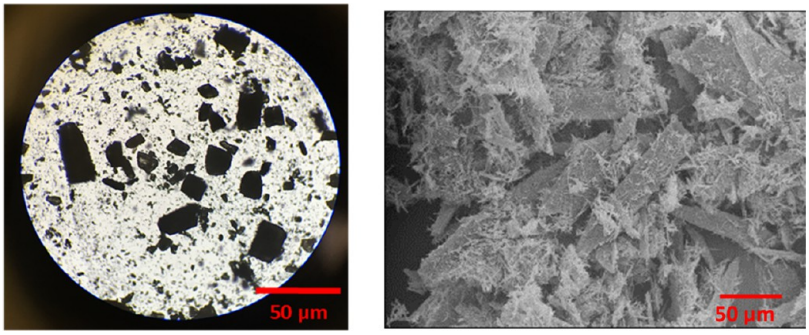

Figure 1. (Left) Microscopic image of the active ingredient (AI) used for the experiments. The finest particles are impurities. (Right) Same sample imaged with scanning electron microscopy.

like crystals, which could be more easily filtered in the form of agglomerates. In this way, spherical agglomerates can be produced without the need to introduce a bridging liquid or additional additives into the solution.[14−17] Liquid−liquid phase separation could also be used to control the crystalline structure[18] of the particles nucleated or to obtain unique crystal morphologies.[19,20]

While the principle of spherical agglomeration through addition of an immiscible bridging liquid is well-known[21−24] and characterized,[25,26] it is less clear how to effectively use the oiling out phenomenon to produce agglomerates with the desired properties. The lack of detailed phase diagrams and fundamental understanding of the physical interactions among the different phases (the two liquids and the solid) during oiling out is the reason why liquid−liquid phase separations are seldom exploited to produce agglomerates.

Process analytical technologies (PAT) tools can be a valuable option for the study of complex multiphase and multicomponent systems that appear as a result of oiling out. PAT tools such as in situ imaging, attenuated total reflectance spectroscopy, or laser backscattering are commonly used to monitor and control both batch and continuous crystallization processes.[3,27,28] Some examples of the use of PAT tools to investigate oiling out phenomena are present in the literature;[17,29−31] however, these studies are limited to the identification of the temperature of liquid−liquid phase separation and the detection of crystal nucleation or agglomeration during cooling. A reason for this limited use of PAT tools might be the fact that the main techniques used for monitoring crystallization processes are not designed to deal effectively with more than two different phases: laser backscattering cannot distinguish droplets from solid particles or agglomerates, attenuated total reflectance probes are not designed to work with some specific dispersed systems, and in situ imaging might not provide clear images, particularly in very dark or concentrated suspensions.

To understand complex phenomena such as oiling out followed by agglomeration, it is necessary to use a PAT-based approach that combines and integrates signals from multiple complementary online measurements.[32]

The aim of this work is to develop such an integrated approach for the study of the thermodynamic and kinetic behavior of partly immiscible ternary phase mixtures. The thermodynamic phase diagram as well as the effects of concentration and temperature on agglomeration were evaluated here using a combination of in situ imaging, laser backscattering, and attenuated total reflectance Fourier transform infrared spectroscopy (ATR-FTIR). Results of dynamic experiments (heating and cooling) were then critically compared and validated with the observation of ternary mixtures at equilibrium conditions. In particular, this work focuses on understanding the interactions among the different phases during both heating and cooling operations. The approach presented can enable a faster and better understanding of both thermodynamic and kinetic aspects of the oiling out and crystallization processes, which are essential for the correct design of robust industrial crystallization processes with precise control over the purity as well as the size and shape distribution of the crystals.

The model compound used for this work is a real active ingredient (AI) provided by the agrochemical company Syngenta (Jealott's Hill R&D, U.K.); this substance was chosen as it showed oiling out and rheology problems during manufacturing. The novel experimental framework developed in this work could be used to gain thermodynamic and kinetic information of other industrial systems presenting problems with oiling out. Results on the AI also showed how liquid−liquid phase separation affects particle agglomeration; this knowledge could be eventually used to develop crystallization processes that allow the formation of spherical agglomerates without the need of adding further compounds or a bridging liquid.

MATERIALS AND METHODS

The organic active ingredient (AI) used for all of the experiments presented here was donated by Syngenta Jealott's Hill International Research Centre (U.K.). The AI crystals had needle-shaped morphology and a broad size distribution due to the presence of impurities, as shown in Figure 1. The total purity of the starting material was around 96%. Mixtures of acetone (purity ≥ 99%, Fisher Scientific) and purified water from a Milli-Q apparatus (Merck) were used as solvents for all of the experiments.

Equilibrium Experiments for Phase Diagram Mapping. Equilibrium experiments were carried out to obtain a thermodynamic map of the ternary phase system of the AI, acetone, and water at different temperatures. Mixtures of 10 g of different ratios of acetone, water, and AI were prepared in centrifuge tubes and inserted in the Radleys Carousel system of parallel stirred reactors (Radleys chemicals). Concentrations of the AI of 10, 20, 30, and 40 g/100 g solution were used in mixtures of acetone and water. The concentrations of acetone used for each AI concentration were 10, 20, 30, 35, 40, 45, 50, 55, 60, and 70 g/100 g solution. Samples were then heated up while stirring and left to equilibrate at a constant temperature for a few hours. After being allowed to settle for 10−15 min,

https://doi.org/10.1021/acs.iecr.2c03494
Ind. Eng. Chem. Res. 2022, 61, 18514−18529

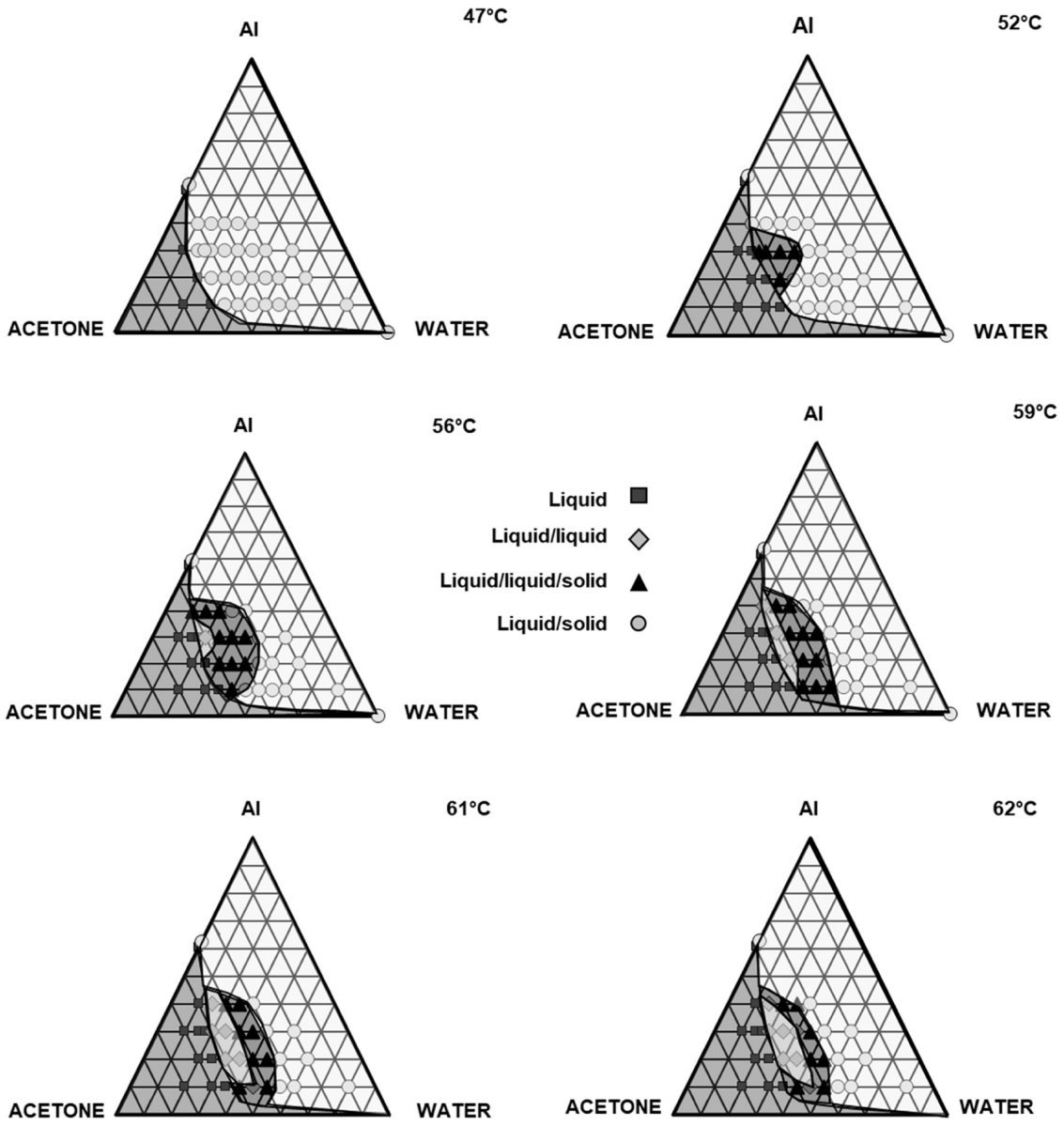

Figure 2. Ternary phase diagrams for mixtures of AI, acetone, and water at different temperatures. Light gray dots indicate liquid and solid mixtures, gray squares represent clear liquid solutions, black triangles are mixtures of solid and two liquid phases, while medium light gray diamonds indicate mixtures of two liquid phases. All data refer to weight fractions of materials. The regions of different phases were qualitatively highlighted in different colors.

each tube was visually inspected to qualitatively assess the number of liquid and solid phases. Samples with the presence of solid aggregates were considered three phase systems; however, the precise phase boundary is approximate. Temperatures of 47, 52, 56, 59, 61, and 62 °C were used to limit evaporation and/or boiling of the solvent. The solubility of the AI in pure acetone and water at the temperatures of interest was also measured gravimetrically using the same procedure reported by Tyson et al.[33]

Crystalline Experiments. Oiling out of the AI in different mixtures of acetone and water was also investigated by in situ imaging using the Crystalline equipment (Crystallization Systems, Technobis). Four grams of mixtures were prepared in 8 mL vials equipped with overhead stirring and loaded into the equipment at ambient temperature. The temperature of the vials was then increased at a rate of 0.2 °C/min until complete dissolution of the solid. Images were collected every minute. Samples were kept at the highest temperature for 15 min and then cooled down to 15 °C at a rate of −0.2° min. Turbidity measurements were also recorded throughout the experiments but this measurement was found to be less reliable than the images. To obtain clear images, mixtures were limited to a maximum AI content of 10% w/w for these experiments. Table SI1 shows the exact ratios used for the experiments and the temperatures of interest for each sample analyzed.

The Crystalline can provide useful information only at these low amounts of dispersed solids and for fairly clear (low AI concentration) solutions. Subsequent experiments were performed in the EasyMax platform using the PAT tools to probe higher concentration of AI, allowing the study of ternary mixtures with compositions along the whole liquid−liquid region.

EasyMax Experiments. The behavior of mixtures of AI, water, and acetone during heating and cooling was investigated

https://doi.org/10.1021/acs.iecr.2c03494
Ind. Eng. Chem. Res. 2022, 61, 18514−18529

over a broader composition range using the Mettler Toledo EasyMax 102 platform equipped with a Particle Track G400 and a ReactIR 15 with 9.5 mm AgX Dicomp immersion probes (all Mettler Toledo). The iControl software (Mettler Toledo) was used to control the temperature and stirring rate in the 100 mL reactor used for the experiments. Laser backscattering and IR spectroscopy data were collected using the ic FBRM and iC IR software (Mettler Toledo). These two techniques were respectively used to collect qualitative information on the suspended particles (via laser backscattering) and the solution chemistry (attenuated total reflectance FTIR spectroscopy). Laser backscattering data were collected every 10 s, while ATR-FTIR spectra were collected every minute. Different mixtures of AI, acetone, and water (100 g in total) were prepared and loaded into one of the two EasyMax reactors. Overhead stirring (300−500 rpm) was used for all experiments and a vertical condenser was fitted on top of the reactor to minimize pressurization and solvent loss. A heating rate of 0.3 °C/min or slower was used for all mixtures and the final temperature was maintained for 15−20 min for equilibration. Cooling at −0.1 °C/min was then performed. Samples were periodically collected from the reactor during the experiments to visually inspect the system and check the presence of agglomerates and oiling out. Furthermore, occasionally, the stirring was stopped and the vessel was taken out of the EasyMax case for visual inspection. In case of suspected fouling of the probes (e.g., spikes in the chord length distributions, CLD), these were taken out of the vessel and cleaned carefully with acetone and a tissue.

Details of the mixtures used for this set of experiments are shown in Table SI2.

Data were processed using the dedicated Mettler Toledo software as well as Excel 2016 and Matlab R2021a. All spectra were smoothed using the Savitzky−Golay filter (15 points, second-order polynomial). To better visualize the changes in IR spectra, the first derivative of each spectrum was calculated to remove any baseline shift and to partly deconvolute overlapping peaks. The intensity of a specific AI first derivative peak (at 1672 cm^{-1}) was estimated for each measurement and monitored over time during dynamic heating and cooling experiments.

RESULTS AND DISCUSSION

Equilibrium Experiments and Ternary Phase Diagram. The results from the equilibrium experiments are shown in Figure 2, in the form of ternary phase diagrams at different temperatures. Although acetone and water are miscible in all proportions and at any temperature, the presence of the AI induces a liquid−liquid separation at high temperatures and intermediate water and acetone concentrations. The AI solubility in water is almost zero at all temperatures tested; however, it reaches over 60 g/100 g solution in acetone above 60 °C. This higher affinity with acetone compared to water can also explain why the AI powder was very hydrophobic and could not be effectively wetted by water, as observed experimentally. Above 50 °C, a liquid−liquid separation can be observed for some mixtures. As the temperature is raised, the solid−liquid region (in light gray dots) is increasingly replaced by a solid−liquid−liquid and then a liquid−liquid region as the AI is dissolved. The liquid−liquid region emerges at lower temperatures at intermediate ratios of AI to water, and then progresses to cover the majority of the possible ratios as the temperature increases. Only the extremes of AI and water ratios lead to a conventional solid−liquid phase boundary across all temperatures, defining a limited region where a liquid−liquid separation could be avoided.

Figure 3A−E shows the phases that are formed in ternary mixtures of AI, acetone, and water at high temperature: an aqueous liquid (transparent, low density) and an organic liquid (dark brown, high density) that contains most of the acetone and AI.

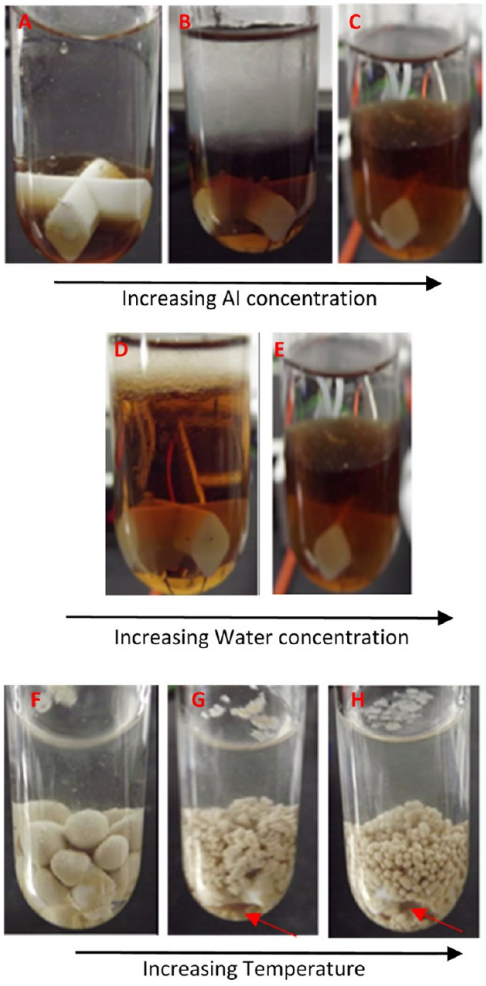

Figure 3. Effect of temperature and increase in the concentration of AI and water on ternary mixtures of AI, acetone, and water. Increasing volume fraction of the organic phase at AI concentration of (A) 10% w/w, (B) 20% w/w, and (C) 30% w/w in solvent mixtures of 56−57% w/w acetone in water above 60 °C. As the AI concentration increases, the volume fraction of the organic liquid becomes higher. Increasing volume fraction of the water phase for mixtures of 30% w/w AI at 64 °C and acetone concentration in the solvent of (D) 71% w/w and (E) 57% w/w. As the water in the solvent increases, the volume fraction of the aqueous liquid increases. Formation of agglomerates in a mixture of 20/35/45 w/w AI/acetone/water at (F) 59, (G) 61, and (H) 62 °C. The size and strength of the agglomerates depend on the amount of AI dissolved and the volume fraction of the organic liquid phase; as the temperature is raised, both of them increase.

It is worth noticing that, depending on the composition of the mixture and the temperature, different volume ratios of the aqueous and organic liquids can form (further details can be found in Table SI3). The two liquids could be easily

https://doi.org/10.1021/acs.iecr.2c03494
Ind. Eng. Chem. Res. 2022, 61, 18514−18529

distinguished in the equilibrium experiments as they presented two different colors and densities. The organic liquid, rich in acetone and AI, had a dark brown color and a higher density than the aqueous phase (as shown in the photos of Figure 3). The aqueous phase is transparent and low in density; additionally, due to the AI hydrophobicity, this phase does not interact with the suspended solid particles.

The volume ratio between the two liquid phases is an important parameter as it will influence which of the two phases is the dispersed one upon mixing: emulsions of the organic liquid in the aqueous phase or vice versa are obtained if one of the two phases is in much lower volume fraction than the other (e.g., the organic phase is the dispersed one in the system shown in Figure 3A, and the continuous one for the system shown in Figure 3D). Since the AI is mostly dissolved in the organic liquid, the ratio between the two liquid phases will affect where nucleation happens (continuous or dispersed phase) as well as the agglomeration process, as shown in more details in the next experimental sections.

In the equilibrium experiments, the presence of solid agglomerates was observed in several samples as the temperature was increased, as shown in Figure 3F−H. The formation of these agglomerates is associated with the liquid−liquid separation. In fact, while AI particles are not easily wettable by the aqueous phase, they are seen to have greater affinity for the organic liquid; this phase can act as a bridging liquid to enable particle agglomeration. This hypothesis is also corroborated by the fact that, as the temperature is raised and the amount of organic liquid increases with simultaneous dissolution of the solid, the agglomerates become smaller and weaker as the ratio of solid to organic liquid decreases (Figure 3F−H). Such behavior is typical of spherical agglomeration processes, where the ratio between the dispersed solid and the amount of bridging liquid determines the strength and size of the agglomerates formed.[24] From a practical point of view, it is worth noticing that the detection of the organic liquid phase in the presence of solid particles and/or agglomerates was not trivial. Nevertheless, a change in the composition of the continuous solution could be observed by a reduction in the intensity of the color of the liquid solution, indicating that the AI has left the continuous phase and an oil phase has formed.

The phase diagram defines the regions where thermodynamic phase separations occur. However, during cooling crystallization, clear solutions can cross a region of metastability before nucleation where kinetic oiling out is possible. This phenomenon will be described more in details in the final sections of this work.

Dynamic Heating Experiments with In Situ Imaging. Imaging is a very powerful tool for the detection of liquid−liquid phase separations during heating up of slurries, as it can distinguish between particles and droplets. For the experiments conducted with the Crystalline platform compositions of 5/43/52, 7/42/51 and 10/40/50 w/w AI, acetone, and water were chosen. The samples analyzed have similar solvent composition and increasing amount of AI, which was still kept below 10% w/w to obtain clear images. Figure 4 shows images obtained with the crystalline platform during the experiments.

As the temperature of these relatively diluted mixtures is increased, solid particles start to agglomerate due to the presence of a small amount of the organic liquid phase. While the amount of this liquid phase increases and the suspended particles are depleted, as a result of an increase in temperature and further dissolution of AI, agglomerates lose their strength

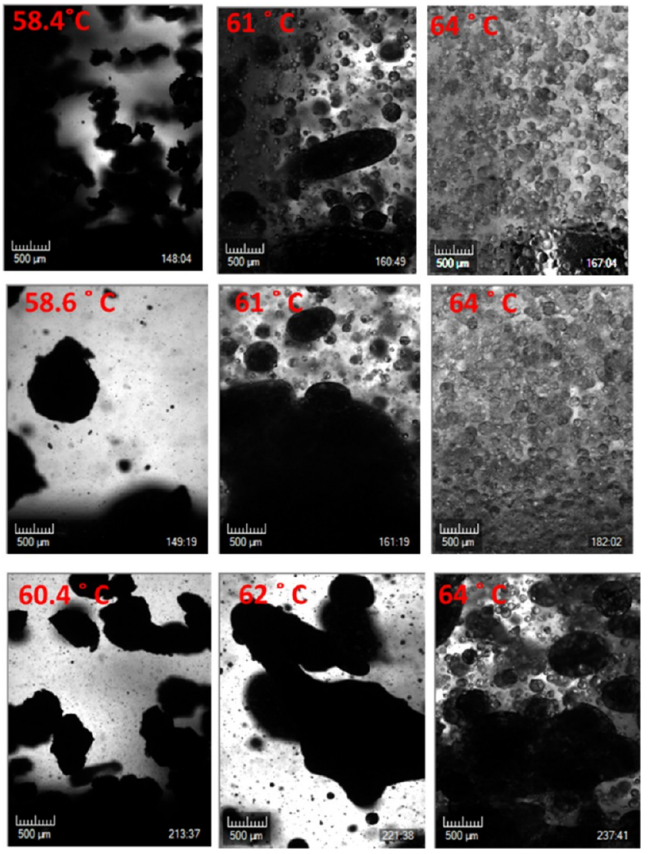

Figure 4. Crystalline images of mixtures of AI/acetone/water of concentrations 5/43/52 w/w (first line), 7/42/51 (second line), and 10/40/50 (third line).

and free droplets of the organic liquid become visible in suspension. It is evident from the images that the organic liquid has great affinity for the solid AI and forms large liquid domains containing particles that are dispersed in a clear aqueous phase. When the solid particles are fully dissolved, a fine emulsion of the organic liquid in the aqueous phase is obtained. Fine droplets are obtained at 64 °C upon complete dissolution of the solid particles for 5/43/52 and 7/42/51 w/w AI, acetone, and water mixtures. For the final sample at 10/40/50 w/w, complete dissolution of the solid was not achieved at 64 °C; hence, large domains of organic liquid wetting the residual particles are still visible at this temperature.

Dynamic Heating Experiments with Laser Backscattering and ATR-FTIR In Situ Spectroscopy. In this section, the transition from solid−liquid to solid−liquid−liquid and then to liquid−liquid systems was studied in suspensions at high solid concentrations.

Figure 5 shows the three chosen experimental points in the phase diagram, which are mixtures of 10/40/50 (pink star), 20/40/40 (orange star), and 40/45/15 (yellow star) w/w of AI in acetone and water. While the acetone concentration remains fairly constant among the three points, varying the ratio between AI and water allows different volume ratios of the two immiscible liquids to be achieved. At higher concentrations of AI (the top left of the liquid−liquid region of Figure 5), the organic liquid is predominant and will constitute the continuous phase, while the aqueous liquid is dispersed. At lower concentrations of AI and higher water content, the organic liquid is dispersed in the aqueous phase.

https://doi.org/10.1021/acs.iecr.2c03494
Ind. Eng. Chem. Res. 2022, 61, 18514−18529

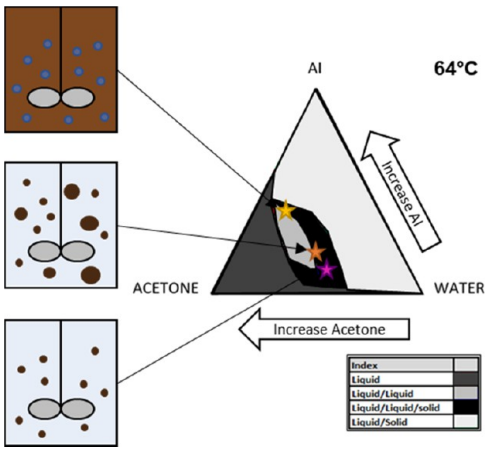

Figure 5. Qualitative representation of different ternary mixtures upon complete dissolution, including their position in the phase diagram. The water-rich phase is represented in blue, while the organic phase is represented in brown. The increase in acetone and AI both induce an increase in the organic phase at the dispense of the aqueous one.

Figure 6a shows the laser backscattering and ATR-FTIR data collected during heating of the ternary mixture of 10/40/50 w/w of AI in acetone and water. This mixture generates a liquid−liquid separation above 59 °C, based on the phase diagram of Figure 2, and has a high amount of solid that does not fully dissolve below 62 °C. Furthermore, a direct comparison with the results shown in the previous section is possible, as this concentration could be tested with the crystalline setup.

The disappearance of solid particles during heating is evident from the decrease in the total counts recorded by laser backscattering. Particles with smaller chord length dissolve earlier than larger ones, as shown by the decreasing trends for the small (10−100 μm) and coarse (>100 μm) counts in Figure 6a and by the trend of the mean of square weighted CLD (SWCLD). The disappearance of small particles is due to both dissolution and agglomeration. The trends for the number of counts over time do not show direct evidence of agglomeration; however, the formation of particle agglomerates can be detected via observation of the chord length distributions (CLD) over time. In fact, Figure 6c shows an increase in the number of larger chord lengths upon heating from 45 to 56 °C that must be due to agglomeration. These agglomerates then quickly dissolve at temperatures above 56 °C as a result of further dissolution of the AI. It is noteworthy that in some ternary mixtures, agglomerates formed early on during the heating profile and were of large size (>100 μm); in such cases, a significant increase in the number of counts for coarse particles was observed before deaggregation and particle dissolution (see Figure SI1).

The formation and dispersion of droplets of the organic liquid can be clearly observed in Figure 6a at around 58 °C, when the number of counts for particles of all chord length starts increasing again. At the same temperature, it is also possible to observe the formation and growth of a peak in the CLD at smaller values compared to the starting solid materials and agglomerates, indicating the formation of fine droplets whose size distribution changes with temperature (as shown in Figure 6c).

Figure 6a also shows the intensity of the AI peak at 1672 cm^{-1} of the first derivative of ATR-FTIR spectra. This value shows a sudden increase at 58 °C and then a sharp decrease before the end of the heating profile. As shown in Figure 6b, which pictures a wider region of the FTIR spectrum, this increase in intensity is recorded for most of the peaks in the 1600−1700 cm^{-1} region, indicating a sudden increase in the solute concentration of the sample. However, Figure 6a,c shows that these changes in intensity disappear above 60 °C. This behavior is likely related to the oiling out process.

In fact, as shown in the Crystalline images of Figure 4, large domains of organic liquid appear when solid particles and organic disperse liquid droplets coexist. These liquid domains possibly stick to the ATR probe, disturbing the signal and causing the observed changes in the FTIR spectra. As the solid progressively disappears, the droplets of organic liquid become more uniformly dispersed in the continuous phase; this event can be observed in the increase in small counts above 59 °C, as shown in Figure 6c. Smaller droplets are less likely to impact the ATR prism and influence the measurement; hence, the FTIR signal goes back to measuring only the continuous aqueous phase.

The formation of agglomerates, which is detected above 46 °C for this experiment, indicates that this mixture has entered the solid−liquid−liquid region. This temperature is considerably lower than the one detected in the equilibrium experiments (59 °C as shown in Figure 2), suggesting that laser backscattering is to a certain extent able to detect this thermodynamic phase transition for an agglomerating mixture. For this type of mixtures, this technique is also more efficient than both in situ imaging and visual inspection, which was performed during the equilibrium experiments. In fact, due to high solid concentration, it was not possible to clearly detect the presence of small agglomerates or dispersed liquid droplets during the equilibrium experiments, and the Crystalline images at 46 °C for this mixture were too crowded with particles to clearly show the presence of dispersed liquid droplets.

More challenging though is the accurate detection of the liquid−liquid region with any PAT tool. It is difficult to determine when the solid completely disappears as, just before dissolution, deagglomerated particles coexist with dispersed droplets of similar size and color. However, an approximate point of complete dissolution can still be identified. In fact, deagglomerated particles tend to be wetted by the organic liquid and form large biphasic domains; the disappearance of these domains and the redispersion of small droplets of organic liquid can be approximately considered as the liquid−liquid region boundary.

The determination of this event is relatively easy with in situ imaging but also laser backscattering can provide an indication of it. The 10/40/50 w/w mixture, in particular, still presented solids at 64 °C as demonstrated by the presence of large biphasic domains shown in Figure 6, and by the high counts of coarse particles (>100 μm) in laser backscattering. Hence, the liquid−liquid boundary is at a higher temperature, in agreement with the equilibrium experiments (Figure 2).

Moving along the constant acetone boundary toward a higher organic liquid fraction, the ternary mixture 20/40/40 w/w AI, acetone, and water showed similar trends to the 10/40/50 w/w mixture but with more evident formation of agglomerates, as it can be observed in Figure SI1. The dispersed phase for this mixture is still the organic liquid, but its volume fraction is higher compared to the 10/40/50 w/w

https://doi.org/10.1021/acs.iecr.2c03494
Ind. Eng. Chem. Res. 2022, 61, 18514−18529

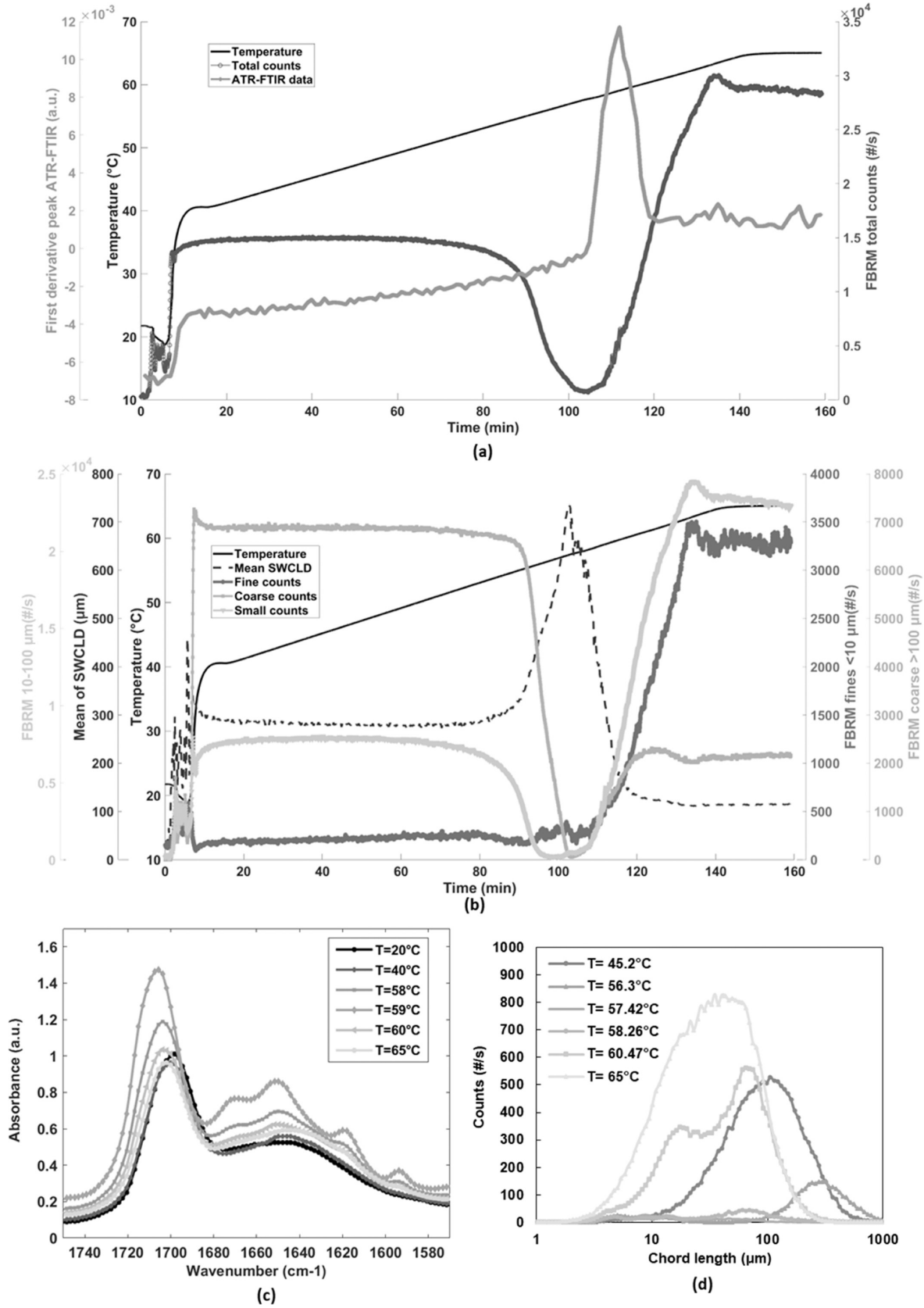

Figure 6. Data from laser backscattering and ATR-IR spectroscopy collected in a mixture of 10/40/50 w/w AI, acetone, and water heated at 0.2 °C/min. (a, b) Laser backscattering trends calculated from macro distributions exported from the instrument and intensity of 1672 cm^{-1} in the first derivative and smoothed spectra, (c) ATR-FTIR spectra collected at different temperatures during heating, and (d) CLDs from laser backscattering collected during heating.

https://doi.org/10.1021/acs.iecr.2c03494
Ind. Eng. Chem. Res. 2022, 61, 18514−18529

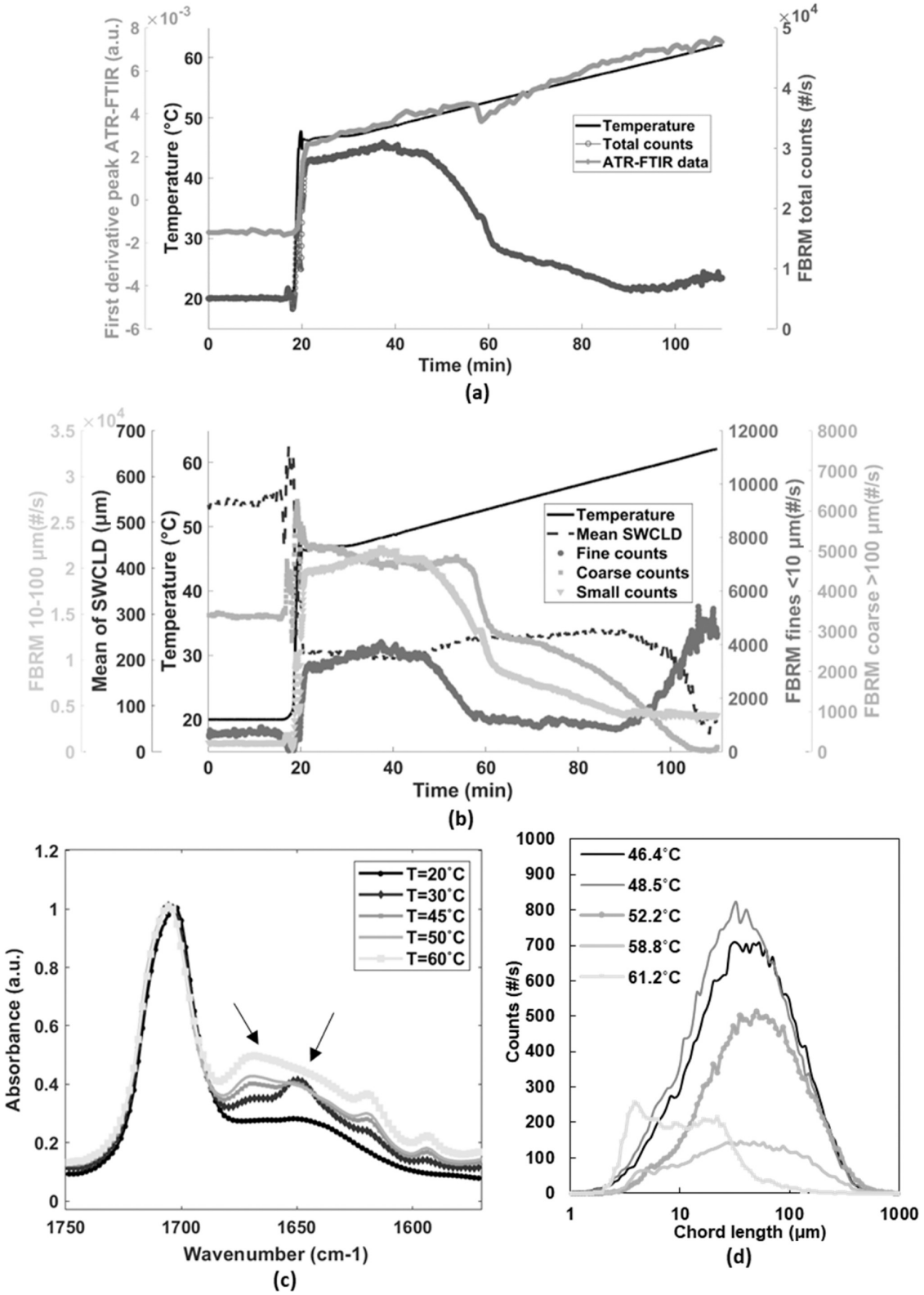

Figure 7. Data from laser backscattering and ATR-IR spectroscopy collected in a mixture of 40/45/15 w/w AI, acetone, and water heated at 0.2 °C/min. (a, b) Laser backscattering trends calculated from the macro distributions exported from the instrument and intensity of the 1672 cm^{-1} in the first derivative and smoothed spectra, (c) ATR-FTIR spectra collected at different temperatures during heating, and (d) CLDs from laser backscattering collected during heating.

mixture. The trends for SWCLD, the small and fine counts are similar to those observed in the 10/40/50 w/w mixture; however, a clear increase in the number of coarse particles associated with the formation of agglomerates is evident. Hence, for this mixture, the liquid−liquid phase separation is easily detected as the temperature of formation of agglomer-

https://doi.org/10.1021/acs.iecr.2c03494
Ind. Eng. Chem. Res. 2022, 61, 18514−18529

ates, and this measurement is more accurate than that observed in the equilibrium experiments (around 50 °C instead of 56 °C). The evident droplet coalescence and the increase in the coarse counts between 56 and 58 °C might be related to the formation of domains of organic liquid and wetted solid particles, resulting from deagglomeration. The gradual disappearance of such domains between 59 and 63 °C is in good agreement with the equilibrium experiments, which revealed a dissolution temperature of about 63 °C. Figure 7 shows the laser backscattering and ATR-FTIR data for the heating of a mixture of 40/45/15 w/w AI, acetone, and water. In contrast to the previous two mixtures, upon complete dissolution of the solid, this system forms a dispersion of the aqueous phase within the organic liquid. In the equilibrium experiments (see phase diagram of Figure 2), the oiling out for this ternary mixture was first detected at 56 °C, with full dissolution of the solid particles above 61 °C. No visible formation of agglomerates is observed from the laser backscattering data, and the intensity of the FTIR peak of interest (first derivative at 1672 cm^{-1}) does not present any spike associated with sticking of the dispersed phase on the probe. Nevertheless, as shown in Figure 7c, a change in the composition of the continuous phase due to oiling out is evidenced by a sudden increase in the ratio between the intensities of the 1650 and 1670 cm^{-1} peaks (between 45 and 50 °C).

No agglomeration is detected and the formation of a discrete dispersed phase is indicated both by an increase in the number of small counts starting above 58 °C and by the formation of a secondary CLD peak below 10 μm. Nevertheless, liquid droplets probably start forming before this increase in counts; in fact, it is possible to notice a change in the rate of decrease of all counts between 52 and 58 °C. This trend is very likely due to the formation of organic liquid droplets that coexist in a nonaggregated form with the dissolving particles.

The ATR-FTIR spectra also confirm this hypothesis as the change in the composition of the continuous phase occurs in this temperature range (Figure 7b). Eventually, the solid particles are all dissolved and the formation of droplets prevails: this is not precisely detectable with laser backscattering but it probably happens between 61 and 62 °C when the counts of coarse particles approach zero, in accordance with the equilibrium experiments.

Hence, for this experiment, PAT tools allowed the determination of both liquid−liquid phase separation and complete dissolution of the solids. Nevertheless, it is worth noticing that having a good understanding of the ternary phase diagram is essential to rationalize the laser backscattering and spectroscopic data collected during heating experiments.

Dynamic Heating Experiments—Mechanism of Agglomeration, Disaggregation, and Droplet Dispersion. From the EasyMax data shown in the previous section, it is clear that agglomeration tends to happen in ternary mixtures where the organic liquid is the disperse phase (e.g., heating up of the 10/40/50 and 20/40/40 w/w mixtures presented earlier), which can wet the AI particles much more effectively than the aqueous phase. A schematic summary of the mechanism of agglomeration/deagglomeration during heating is shown in Figure SI2, together with images of AI agglomerates collected with scanning electron microscopy.

The ratio between the volume of dispersed organic liquid and solid particles strongly affects the mechanism of liquid−liquid phase separation and agglomeration. Hence, ternary mixtures with different values of such solid to liquid ratio were further studied in this section.

The concentrations used for this set of experiments are shown in Figure 8: the AI content was either 10 or 20% w/w, while the acetone concentration in the solvent ranged between 44 and 55% w/w.

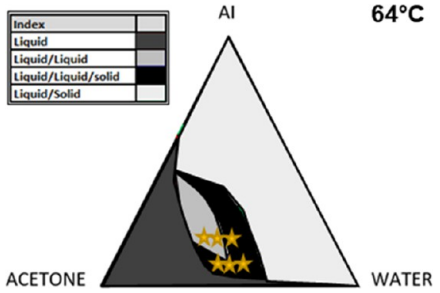

Figure 8. Ternary phase diagram at 64 °C. Yellow stars represent the concentrations used for the laser backscattering experiments designed to investigate agglomeration.

These mixtures go through oiling out upon heating and sit in the region of the phase diagram where the dispersed phase is the organic liquid, which has high affinity with the solid particles. For all concentrations at 10% w/w of AI and for the lowest acetone level of 20% w/w AI (20/35/55 w/w AI, acetone, and water mixture), the volume fraction of the organic liquid is much lower than that of the aqueous phase. However, the volume fractions of the organic and aqueous phases after dissolution of AI for 20/40/40 and 20/45/35 w/w are similar, as shown in Table SI3.

Figure 9 shows the evolution of the CLD recorded from laser backscattering for this set of experiments. For example, upon heating from 45 to 56 °C, the 20/40/40 w/w mixture showed a reduction of the total counts and a shift of the CLD to higher chord lengths. At 58 °C, the total number of counts decreased due to sedimentation of large agglomerates. At this temperature, the CLD also shifted back to lower counts and two peaks can be noticed in the distribution. These are associated to the droplets of the disperse organic liquid forming, as well as the residual solids in suspension. Oiling out proceeded up to 60 °C, generating an increase in the number of counted droplets. The bimodal CLD is related to the forming droplets together with the deagglomeration phenomena previously discussed. At 65 °C, the solid was fully dissolved, and hence the measured CLD corresponds to the disperse liquid phase only.

When comparing the extent of agglomeration among different compositions, quantified as a shift of the CLD to higher chord length values, it can be observed that this is higher when increasing the AI content at a fixed solvent composition. The 10/45/45 and 10/50/40 w/w mixtures do not show significant agglomeration, which is instead observed in the 20/40/40 and 20/45/35 w/w mixtures. The 20/35/25 w/w presented more and larger agglomerates than the 10/40/50 w/w, respectively, 107 #/s against 73 #/s for a chord length of 518 μm and a temperature of 56−57 °C (the same stirring rate was used for these experiments). The onset temperatures for agglomeration are 54−55 °C for both the 10/50/40 and 20/35/55 w/w mixtures, lower than the temperatures identified in the equilibrium experiments (59 and 61 °C). For the higher acetone concentration mixture of 20/40/40 w/

https://doi.org/10.1021/acs.iecr.2c03494
Ind. Eng. Chem. Res. 2022, 61, 18514−18529

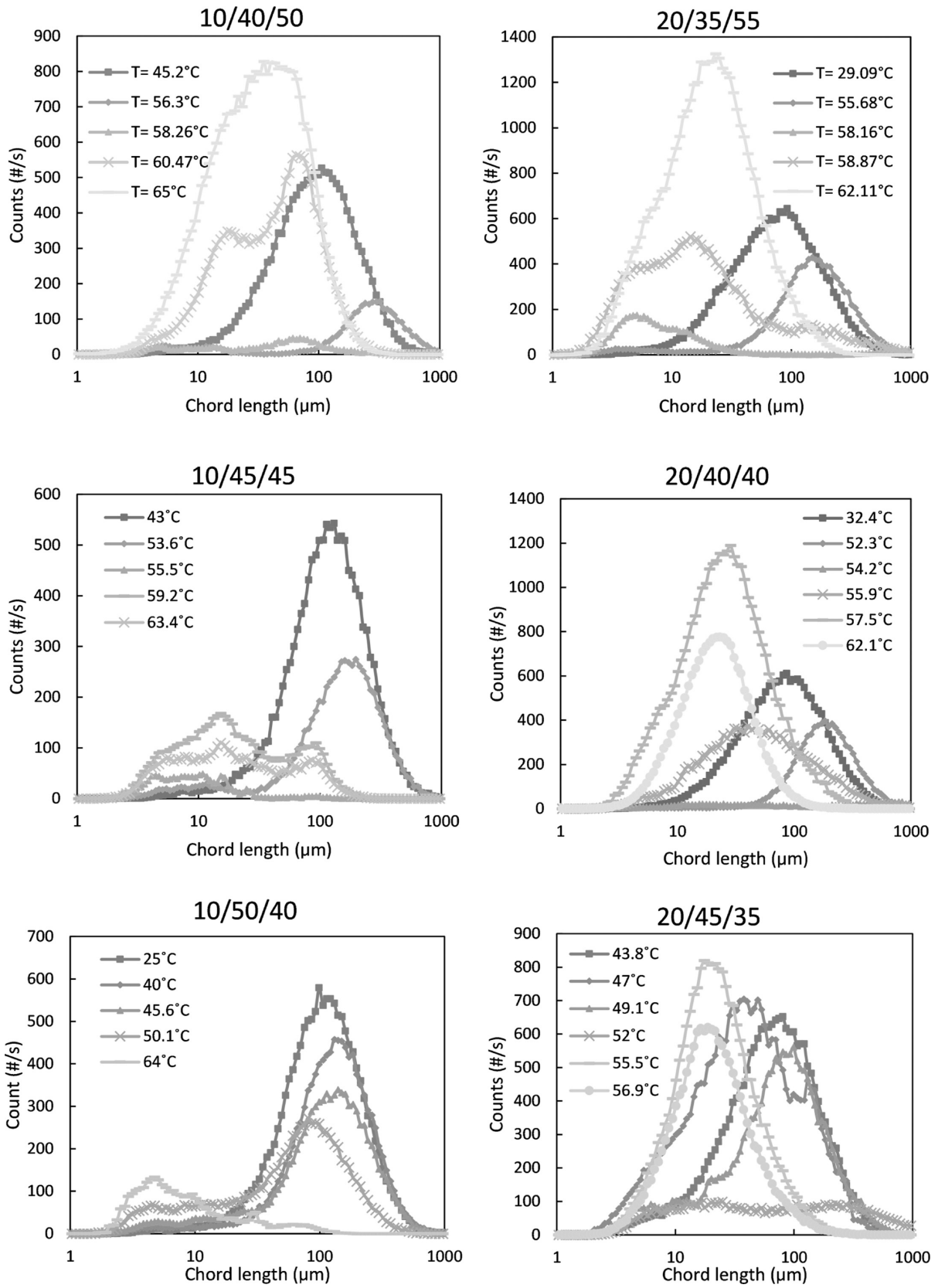

Figure 9. Chord length distributions from laser backscattering for ternary mixtures of AI, acetone, and water (exact w/w concentrations are indicated on top of the figure). Graphs in the same column have same AI amount and increasing concentration of acetone (from top to bottom). Graphs on the same row have the same solvent composition but different AI concentrations.

w, agglomeration is detected at 50 °C, 6 °C lower than the temperature identified in the equilibrium experiment. As the acetone concentration (and hence the AI solubility at a given temperature) increases, the amount and strength of agglom-

https://doi.org/10.1021/acs.iecr.2c03494
Ind. Eng. Chem. Res. 2022, 61, 18514−18529

erates decreases. In fact, a higher amount of AI dissolved in solution means less solid suspended and more organic liquid separated from the initial solution. This is particularly evident when comparing the trends of 20/40/40 and 20/45/35 w/w mixtures. The first mixture shows evident agglomeration followed by deagglomeration and droplet dispersion between 50 and 55 °C. However, the 20/45/35 w/w mixture presented agglomeration and deagglomeration in a narrower range of temperature, between 50 and 52 °C (lower than the liquid−liquid separation temperature of 54 °C identified in the equilibrium experiments). Furthermore, within the agglomeration temperature range, the coarse counts are lower in number for the 20/45/35 w/w mixture than for the 20/40/40 w/w one, about 100 #/s versus 300 #/s for a CL of around 250 μm.

In all mixtures shown in Figure 9, it is possible to identify a region where the total number of counts is very low and the CLD is almost flat. This region precedes deagglomeration and redispersion of droplets of the organic liquid phase. In fact, after reaching such a point, the number of counts increases again and the CLD is shifted to lower chord length values as droplets and residual suspended solid particles are smaller than the agglomerates.

Finally, it is also worth noticing that, even after dissolution of most of the solid particles, the CLD keeps changing while the temperature increases. This is due to changes in the composition and relative mass fraction of the two liquid phases, which are related to the increase in the total area of the liquid−liquid region as the temperature is raised.

A more detailed comparison of the laser backscattering data with the equilibrium experiments is shown in Table SI4, where the temperatures at which events of interest are detected are shown for all mixtures analyzed, not just the ones of Figure 9.

Understanding agglomeration as a function of the composition of ternary mixtures is important for two reasons: (1) to correctly define the phase diagram of ternary mixtures since the onset of agglomeration can, in some cases, be used as an indirect way to detect liquid−liquid phase separation and (2) to exploit this phenomenon during seeded cooling crystallization to produce solids that are easier to handle in the downstream processing.

Cooling Crystallization from Liquid−Liquid Systems. The last two sections of this paper present the behavior of different types of ternary mixtures during cooling crystallization experiments.

Three different scenarios were considered, as schematically shown in Figure 10. Two mixtures at 20/45/35 and 40/45/15 w/w AI, acetone, and water were chosen as representative of crystallization from thermodynamically stable liquid−liquid systems. Upon complete dissolution of the solids, the 20/45/35 w/w mixture is a dispersion of organic liquid droplets within a continuous aqueous phase; however, in the 40/45/15 w/w mixture, the aqueous phase is dispersed in the organic liquid. Finally, the third mixture analyzed is made up of 7/52/41 w/w AI, acetone, and water, and it is a clear homogeneous solution at high temperature. However, due to its proximity to the liquid/liquid region of the phase diagram, within the metastable zone for crystallization, this ternary mixture showed oiling out before the formation of solid crystals.

Figure 11 shows data collected with laser backscattering and ATR-FTIR spectroscopy during cooling of a ternary mixture of 20/45/35 w/w AI, acetone, and water. The high number of counts between 1 and 100 μm at a high temperature indicated

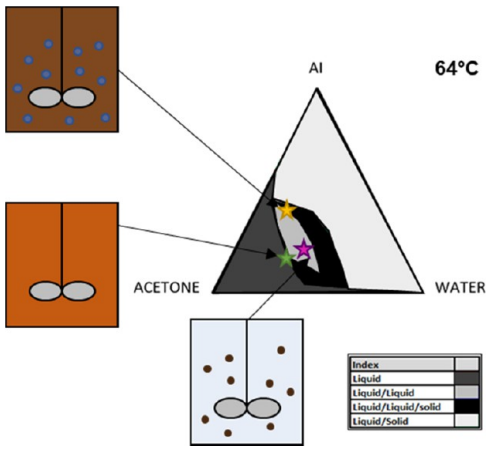

Figure 10. Qualitative representation of the three different ternary mixtures considered for the cooling crystallization experiments. The yellow star represents a 40/45/15 w/w AI, acetone, and water mixture, which is a dispersion of aqueous droplets in the continuous organic liquid upon solid complete dissolution. The pink star is a mixture of 20/45/35 w/w AI, acetone and water, and at a high temperature is a dispersion of organic liquid droplets within a continuous aqueous phase. The composition of the green star is instead 7/52/41 w/w AI, acetone, and water, and this mixture is a clear liquid upon complete dissolution of the solid. However, due to its proximity to the L/L region, it can show metastable oiling out.

that this is a liquid−liquid system. During cooling, only the fine counts (<10 μm) slightly decrease, possibly due to temperature-dependent changes in the interfacial tension between the two liquid phases, which affects coalescence. At around 33 °C, an increase in all counts is observed for all size ranges, starting from the fine counts up to the coarse (>100 μm) ones. Such trends correspond to the nucleation of solid crystals and the formation of large clusters of particles wetted by the organic liquid. Eventually, these clusters start to sediment to the bottom of the vessel due to their large size, as shown by an abrupt decrease in counts at around 30 °C. When all of the organic liquid is depleted, the solid agglomerates remaining from these clusters start to partly disaggregate or break, while crystal nucleation and growth continues. These phenomena result in an increase in all counts. Below 26 °C, the laser backscattering trends and CLDs are typical of a growing population of crystals with some secondary nucleation and/or breakage.

The intensity of the first derivative ATR-FTIR peak of interest is quite noisy during the cooling stage, before the drop in counts registered at around 30 °C. This is possibly due to the persistence of the original dispersed phase that disturbs the ATR signal, in a similar way to what was observed while heating up a mixture of similar composition (as shown in Figure SI1). The exact onset of nucleation is not clear from this technique, although a significant drop in the signal can be identified at around 33 °C, when the counts of fine and small particles increase. However, the moment when all of the organic liquid is depleted is evident as the noise of the signal decreases significantly. After that, the intensity of the ATR-FTIR peak monitored keeps decreasing and then stabilizes to a constant value, as expected during a desupersaturation process at constant temperature.

Figure SI3 shows the cooling stage of a 20/50/30 w/w mixture of AI, acetone, and water, which is also a liquid−liquid system at high temperature. The trends of the laser

https://doi.org/10.1021/acs.iecr.2c03494
Ind. Eng. Chem. Res. 2022, 61, 18514−18529

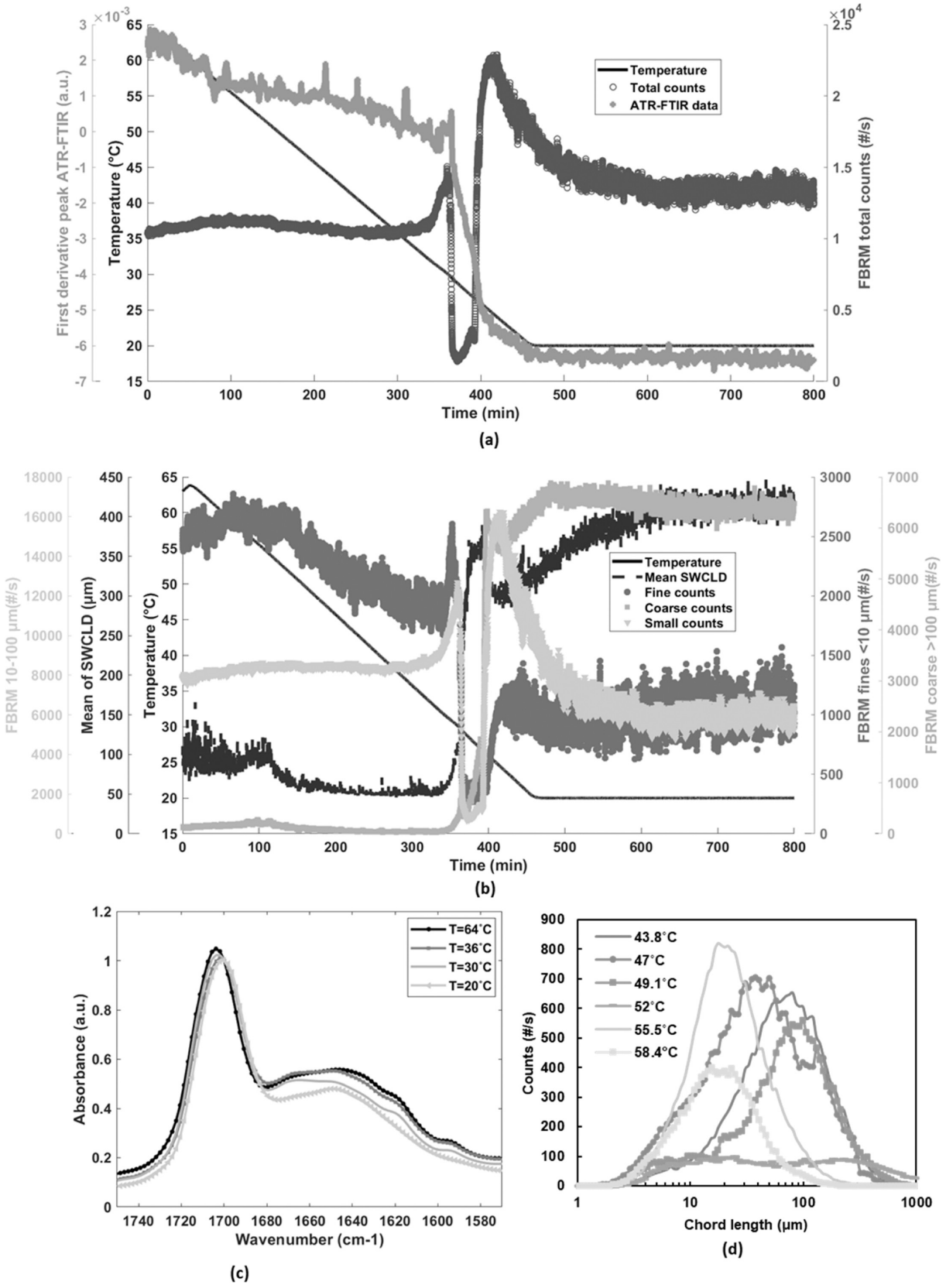

Figure 11. Data from laser backscattering and ATR-IR spectroscopy collected in a mixture of 20/45/35 w/w AI, acetone, and water cooled at −0.1 °C/min. (a, b) Laser backscattering trends calculated from the macro distributions exported from the instrument and intensity of 1672 cm^{-1} in the first derivative and smoothed spectra, (c) ATR-FTIR spectra collected at different temperatures during heating, and (d) CLDs from laser backscattering collected during heating.

https://doi.org/10.1021/acs.iecr.2c03494
Ind. Eng. Chem. Res. 2022, 61, 18514−18529

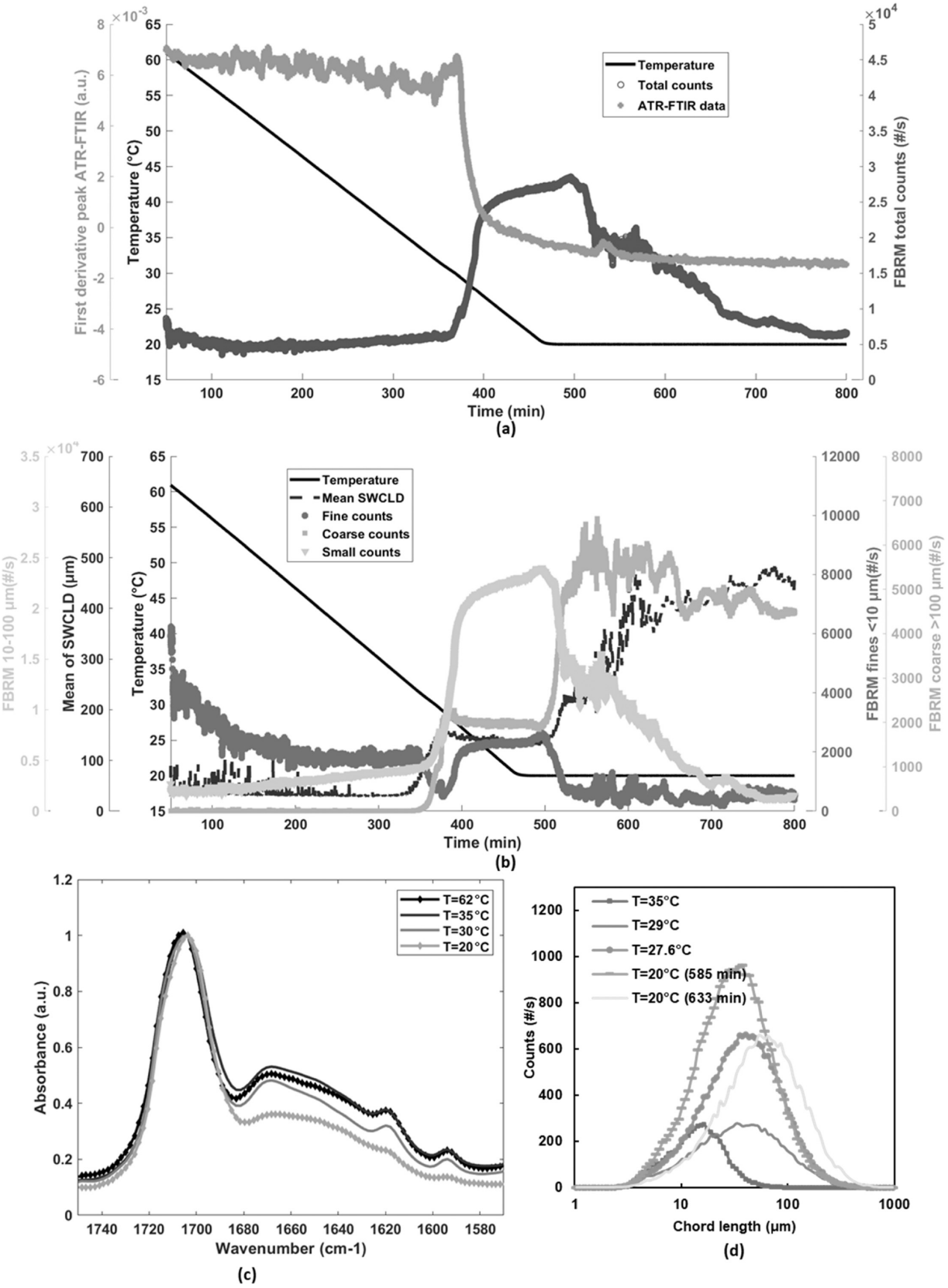

Figure 12. Data from laser backscattering and ATR-IR spectroscopy collected in a mixture of 40/45/15 w/w AI, acetone, and water cooled at −0.1 °C/min. (a, b) Laser backscattering trends calculated from the macro distributions exported from the instrument and intensity of 1672 cm^{-1} in the first derivative and smoothed spectra, (c) ATR-FTIR spectra collected at different temperatures during cooling, and (d) CLDs from laser backscattering collected during cooling.

https://doi.org/10.1021/acs.iecr.2c03494
Ind. Eng. Chem. Res. 2022, 61, 18514−18529

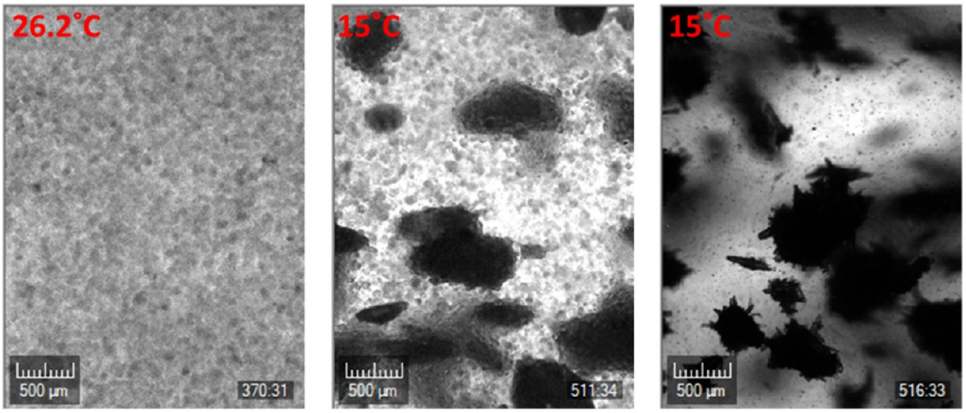

Figure 13. Crystalline images of mixtures of AI/acetone/water of concentrations 7/52/41 w/w.

backscattering signal after crystal nucleation happens are very similar to those shown in Figure 11, with a drop in counts followed by a further increase as agglomeration/disaggregation happens. However, a visible increase in the number and size of the suspended droplets before nucleation of the crystals can be observed. This might be the effect of changes in the relative volume fraction and composition of the two liquid phases associated with the decrease in temperature. In fact, as the temperature is lowered, the liquid−liquid region becomes smaller, affecting the relative mass fraction as well as the AI concentration of the aqueous and organic liquids.

Finally, Figure 12 shows the laser backscattering and ATR-FTIR trends for a mixture of AI, acetone, and water of 40/45/15 w/w. This mixture is a biphasic system at a high temperature where the aqueous liquid is dispersed in the organic one (high acetone and high AI content). In this case, AI crystals nucleate from the continuous phase, which is mixed back with the aqueous liquid as desupersaturation occurs. The agglomeration/disaggregation process observed from previous mixtures is not detected here as the aqueous dispersed phase has lower affinity with the solid compared to the continuous organic liquid. However, some particle agglomeration, not related to oiling out, can be observed after 600 min of the experiment. This phenomenon is most likely due to the high amount of AI contained in this mixture as well as the poor mixing in the EasyMax vessel.

From the experiments shown in this section, it is clear that the mechanisms of nucleation, agglomeration, and disaggregation during cooling crystallization mirror the ones shown during the heating stage. This is shown more clearly in Figure SI4, where both the heating and cooling of the two mixtures analyzed in this section are shown.

Metastable Liquid/Liquid Separation during Cooling Crystallization. While the previous sections described the thermodynamic equilibrium of ternary mixtures of AI, acetone, and water, in this section, the formation of metastable liquid−liquid systems during cooling of a homogeneous liquid phase is presented. It is important to predict metastable oiling out during cooling so that it can be easily prevented by appropriate seeding strategies.

As with laser backscattering, it is not possible to distinguish between droplets and particles, the crystalline was used to precisely detect oiling out during cooling of clear solutions.

Figure 13 shows images from cooling crystallization of a mixture of 7/52/41 w/w AI, acetone, and water. This mixture is a clear solution at a high temperature (64 °C); however, at around 26 °C (supersaturated system), a disperse phase (the organic liquid) is clearly visible. As in this region of the phase diagram, this mixture should be a solid suspension in a single liquid phase, and it can be concluded that the observed droplets belong to a metastable phase. At 15 °C, crystal nuclei start to appear and are initially wetted by the organic liquid; large domains of organic liquid and loose solid particles can be observed. Once the ratio between solid and organic liquid is sufficient, the solid particles dispersed in the organic liquid start to aggregate and form strong agglomerates. Such agglomerates initially coexist with small droplets of organic liquids that are then depleted as the crystals grow. Eventually, all of the organic liquid is depleted and the agglomerates start to partly disaggregate, although their morphology is still considerably different than particles nucleated from a clear solution. Table SI5 shows the temperatures at which oiling out is observed upon cooling of several ternary mixtures that are clear and monophasic at high temperature. There is no clear trend that relates the temperature at which oiling out is observed with the initial composition of clear solution.

CONCLUSIONS

In this work, the thermodynamic and kinetic behavior of ternary mixtures of partially immiscible components were determined using an integrated approach that combined the analysis of signals from in situ imaging, laser backscattering, and ATR-FTIR spectroscopy together with equilibrium experiments and the use of ternary phase diagrams. Such an integrated approach was used to determine the interactions among different liquid and solid phases and allowed more precise estimation of the phase boundaries, particularly liquid−liquid phase separation in ternary mixtures of an AI, acetone and water.

The ternary system studied was found to separate into two liquid phases, an aqueous and an organic one, at certain temperatures and concentrations of the three components. Liquid−liquid separation can be observed in the phase diagram above 50 °C. At higher temperatures, the solid−liquid region of the phase diagram is increasingly replaced by a solid−liquid−liquid and then a liquid−liquid region as the AI is dissolved. This liquid−liquid region emerges at lower temperatures for intermediate ratios of AI to water and then spreads to other ratios as the temperature increases.

The relative ratio among the solid, aqueous, and organic liquid phases was found to govern the interactions among them. In particular, the organic liquid phases behaved similar

https://doi.org/10.1021/acs.iecr.2c03494
Ind. Eng. Chem. Res. 2022, 61, 18514−18529

to a bridging liquid in spherical agglomeration processes, generating strong AI agglomerates in some regions of the phase diagram.

Imaging provided useful information on the mechanism of liquid−liquid phase separation and its kinetic, as well as on the interactions among solid particles and the two immiscible liquids. With this technique it was possible to detect both liquid−liquid phase separation, agglomeration, and solid dissolution. However, imaging was of little use for systems with high solid concentrations or very dark colored solutions. Laser backscattering could not distinguish droplets from solid particles but it could be used to complement the information gained from imaging, to infer when liquid−liquid phase separations occurred and to provide some qualitative data on the mechanism of the dynamics of particle agglomeration/disaggregation. In particular, the onset of agglomeration upon heating could be used as an approximation of the point of liquid−liquid phase separation, regardless of which of the two liquid phases was continuous. Agglomeration could be detected by observation of the CLD, which shifted to higher values during heating, or by an increase in the number of coarse counts coupled with a decrease in the number of suspended fines.

Due to the inability of laser backscattering to distinguish droplets from particles, it was instead not possible to exactly pinpoint the complete dissolution of the solid when agglomeration/disaggregation of the solid particles occurred in the presence of a dispersed liquid phase. A rough estimate of the saturation temperature could instead be gained with laser backscattering when agglomerates were not forming (e.g., the aqueous liquid is dispersed in the organic phase). In this case, the complete dissolution of the solid was indicated by the disappearance of the coarse counts.

ATR-FTIR data could provide some information on changes in the chemical composition of the continuous phase and detect liquid−liquid separation and solid dissolution for mixtures where the aqueous phase was dispersed in the organic liquid. However, in mixtures where the organic liquid was dispersed, the signal was often very noisy, particularly when solid particles were still present.

Cooling crystallization experiments in different multiphase systems (stable or metastable) showed a behavior of crystal nucleation, agglomeration, and disaggregation that mirrored the one observed during heating.

The PAT-based approach proposed here could be adapted to other industrial systems that present complex crystallization processes. Furthermore, the information gained on the mechanism of oiling out followed by crystallization/agglomeration could be eventually used to exploit liquid−liquid phase separation during crystallization processes to produce spherical agglomerates and improve filtration processes.

■ ASSOCIATED CONTENT

Supporting Information

The Supporting Information is available free of charge at https://pubs.acs.org/doi/10.1021/acs.iecr.2c03494.

(1) w/w composition of the mixtures of AI, acetone and water used in the Crystalline experiments, (2) w/w composition of the mixtures used for the Easymax experiments and comparison with data collected during equilibrium experiments, (3) visual information of the disperse and continuous phases at 64 °C as a function of the solvent composition and the AI total content, (4) experimental data from the Easymax experiment for a mixture of AI, acetone and water of w/w ratio of 20/40/40, (5) figure showing schematically the mechanism of formation and disaggregation of AI agglomerates as the temperature of the system is increased, (6) Laser backscattering and ATR-FTIR temperatures of interest from the Easymax experiments and comparison with equilibrium experiments, (7) experimental data from the Easymax experiment for a mixture of AI, acetone and water of w/w ratio of 20/50/30, (8) experimental data from the Easymax experiment for mixtures of AI, acetone and water of w/w ratio of 20/45/35 and 40/45/15, (9) visual information from the Crystalline experiments (PDF)

■ AUTHOR INFORMATION

Corresponding Author

Elena Simone − *Department of Applied Science and Technology, Politecnico di Torino, Torino 10129, Italy; Food Colloids and Bioprocessing Group, School of Food Science and Nutrition, University of Leeds, Leeds LS29JT, United Kingdom;* orcid.org/0000-0003-4000-2222; Email: elena.simone@polito.it

Authors

Gillian Beveridge − *Syngenta Grangemouth Manufacturing Centre, Grangemouth FK3 8XG, United Kingdom*

Pauline Sillers − *Syngenta Grangemouth Manufacturing Centre, Grangemouth FK3 8XG, United Kingdom*

Jennifer Webb − *Syngenta Jealott's Hill International Research Centre, Bracknell RG42 6EY, United Kingdom*

Neil George − *Syngenta Jealott's Hill International Research Centre, Bracknell RG42 6EY, United Kingdom; School of Chemical and Process Engineering, University of Leeds, Leeds LS29JT, United Kingdom*

John Hone − *Syngenta Jealott's Hill International Research Centre, Bracknell RG42 6EY, United Kingdom*

Complete contact information is available at: https://pubs.acs.org/10.1021/acs.iecr.2c03494

Notes

The authors declare no competing financial interest.

■ ACKNOWLEDGMENTS

Funding for this work was provided by the Royal Academy of Engineering (Grant No. IF\192031).

■ REFERENCES

(1) Kim, S.; Johnston, K. P. Molecular Interactions in Dilute Supercritical Fluid Solutions. *Ind. Eng. Chem. Res.* **1987**, *26*, 1206.

(2) (a) Bird, R. B.; Stewart, W. E.; Lightfoot, E. N. *Transport Phenomena*, Wiley: New York, 1960. (b) Bernstein, J. Polymorphism - A perspective. *Cryst. Growth Des.* **2011**, *11*, 632−650. (c) Mullin, J. W. *Crystallization*, 4th ed.; Butterworth Heinemann: Oxford, 2001.

(3) Nagy, Z. K.; Fevotte, G.; Kramer, H.; Simon, L. L. Recent advances in the monitoring, modelling and control of crystallization systems. *Chem. Eng. Res. Des.* **2013**, *91*, 1903−1922.

(4) Klapwijk, A. R.; Simone, E.; Nagy, Z. K.; Wilson, C. C. Tuning Crystal Morphology of Succinic Acid Using a Polymer Additive. *Cryst. Growth Des.* **2016**, *16*, 4349−4359.

(5) Trasi, N. S.; Taylor, L. S. Effect of additives on the crystal growth and nucleation of amorphous flutamide. *Cryst. Growth Des.* **2012**, *12*, 3221−3230.

(6) Vetter, T.; Mazzotti, M.; Brozio, J. Slowing the growth rate of ibuprofen crystals using the polymeric additive pluronic F127. *Cryst. Growth Des.* **2011**, *11*, 3813−3821.
(7) Lafferrère, L.; Hoff, C.; Veesler, S. Study of liquid-liquid demixing from drug solution. *J. Cryst. Growth* **2004**, *269*, 550−557.
(8) Lu, J.; Li, Y. P.; Wang, J.; Ren, G.-B.; Rohani, S.; Ching, C. B. Crystallization of an active pharmaceutical ingredient that oils out. *Sep. Purif. Technol.* **2012**, *96*, 1−6.
(9) Meng, Z.; Huang, Y.; Cheng, S.; Wang, J. Investigation of Oiling-Out Phenomenon of Small Organic Molecules in Crystallization Processes: A Review. *ChemistrySelect* **2020**, *5*, 7855−7866.
(10) Sun, M.; Tang, W.; Du, S.; Zhang, Y.; Fu, X.; Gong, J. Understanding the Roles of Oiling-out on Crystallization of *β*-Alanine: Unusual Behavior in Metastable Zone Width and Surface Nucleation during Growth Stage. *Cryst. Growth Des.* **2018**, *18*, 6885−6890.
(11) Takasuga, M.; Ooshima, H. Control of Crystal Aspect Ratio and Size by Changing Solvent Composition in Oiling Out Crystallization of an Active Pharmaceutical Ingredient. *Cryst. Growth Des.* **2015**, *15*, 5834−5838.
(12) Gao, Z.; Altimimi, F.; Gong, J.; Bao, Y.; Wang, J.; Rohani, S. Ultrasonic Irradiation and Seeding to Prevent Metastable Liquid-Liquid Phase Separation and Intensify Crystallization. *Cryst. Growth Des.* **2018**, *18*, 2628−2635.
(13) Sun, M.; Du, S.; Chen, M.; Rohani, S.; Zhang, H.; Liu, Y.; Sun, P.; Wang, Y.; Shi, P.; Xu, S.; Gong, J. Oiling-Out Investigation and Morphology Control of *β*-Alanine Based on Ternary Phase Diagrams. *Cryst. Growth Des.* **2018**, *18*, 818−826.
(14) Abioye, A. O.; Chi, G. T.; Simone, E.; Nagy, Z. Real-time monitoring of the mechanism of ibuprofen-cationic dextran crystanule formation using crystallization process informatics system (CryPRINS). *Int. J. Pharm.* **2016**, *509*, 264−278.
(15) Schreier, J.; Bröckel, U. Multidimensional separation due to selective spherical agglomeration—Evidence of shape separation via X-ray microtomography. *Particuology* **2021**, *58*, 316−323.
(16) Sun, M.; Shichao, D.; Tang, W.; Jia, L.; Gong, J. Design of Spherical Crystallization for Drugs Based on Thermal-Induced Liquid-Liquid Phase Separation: Case Studies of Water-Insoluble Drugs. *Ind. Eng. Chem. Res.* **2019**, *58*, 20401−20411.
(17) Wang, L.; Bao, Y.; Sun, Z.; Pinfield, V. J.; Yin, Q.; Yang, H. Investigation of Agglomeration in the Presence of Oiling out in the Antisolvent Crystallization Process. *Ind. Eng. Chem. Res.* **2021**, *60*, 4110−4119.
(18) Diez, S. J.; Eddleston, M. D.; Arhangelskis, M.; Milbled, M.; Müller, M. J.; Bond, A. D.; Bučar, D. K.; Jones, W. Crystallization at Solvent Interfaces Enables Access to a Variety of Cocrystal Polymorphs and Hydrates. *Cryst. Growth Des.* **2018**, *18*, 3263−3268.
(19) Yang, H.; Chen, H.; Rasmuson, ÅC. Sandwich crystals of butyl paraben. *CrystEngComm* **2014**, *16*, 8863−8873.
(20) Zhang, X.; Wei, Z.; Choi, H.; Hao, H.; Yang, H. Oiling-Out Crystallization of Beta-Alanine on Solid Surfaces Controlled by Solvent Exchange. *Adv. Mater. Interfaces* **2021**, *8*, No. 2001200.
(21) Chen, M.; Liu, X.; Yu, C.; Yao, M.; Xu, S.; Tang, W.; Song, X.; Dong, W.; Wang, G.; Gong, J. Strategy of selecting solvent systems for spherical agglomeration by the Lifshitz-van der Waals acid-base approach. *Chem. Eng. Sci.* **2020**, *220*, No. 115613.
(22) Cheng, X.; Li, F.; Luo, L.; Ding, Z.; Zeng, L.; Mao, Y.; Huang, X.; Hao, H. On the selection of wetting liquid for spherical agglomeration of cefotaxime sodium. *Powder Technol.* **2020**, *363*, 593−601.
(23) Kawashima, Y.; Okumura, M.; Takenaka, H. Spherical crystallization: Direct spherical agglomeration of salicylic acid crystals during crystallization. *Science* **1982**, *216*, 1127−1128.
(24) Pitt, K.; Peña, R.; Tew, J. D.; Pal, K.; Smith, R.; Nagy, Z. K.; Litster, J. D. Particle design via spherical agglomeration: A critical review of controlling parameters, rate processes and modelling. *Powder Technol.* **2018**, *326*, 327−343.
(25) Peña, R.; Burcham, C. L.; Jarmer, D. J.; Ramkrishna, D.; Nagy, Z. K. Modeling and optimization of spherical agglomeration in suspension through a coupled population balance model. *Chem. Eng. Sci.* **2017**, *167*, 66−77.
(26) Peña, R.; Jarmer, D. J.; Burcham, C. L.; Nagy, Z. K. Further Understanding of Agglomeration Mechanisms in Spherical Crystallization Systems: Benzoic Acid Case Study. *Cryst. Growth Des.* **2019**, *19*, 1668−1679.
(27) Simon, L. L.; Pataki, H.; Marosi, G.; Meemken, F.; Hungerbühler, K.; Baiker, A.; Tummala, S.; Glennon, B.; Kuentz, M.; Steele, G.; Kramer, H. J. M.; Rydzak, J. W.; Chen, Z.; Morris, J.; Kjell, F.; Singh, R.; Gani, R.; Gernaey, Kv.; Louhi-Kultanen, M.; Chiu, M. S.; et al. Assessment of Recent Process Analytical Technology (PAT) Trends: A Multiauthor Review. *Org. Process Res. Dev.* **2015**, *19*, 3−62.
(28) Simon, L. L.; Simone, E.; Abbou Oucherif, K. Crystallization process monitoring and control using process analytical technology. *Comput.-Aided Chem. Eng.* **2018**, *41*, 215−242.
(29) Deneau, E.; Steele, G. An in-line study of oiling out and crystallization. *Org. Process Res. Dev.* **2005**, *9*, 943−950.
(30) Parimaladevi, P.; Kavitha, C.; Srinivasan, K. Investigation of the effect of liquid-liquid phase separation (LLPS) on nucleation and different growth stages of vanillin and bulk growth of defect-free single crystals from aqueous solution-a new approach. *CrystEngComm* **2014**, *16*, 2565−2569.
(31) Yang, H.; Rasmuson, Å. C. Investigation of batch cooling crystallization in a liquid-liquid separating system by PAT. *Org. Process Res. Dev.* **2012**, *16*, 1212−1224.
(32) Simone, E.; Saleemi, A. N.; Nagy, Z. K. In situ monitoring of polymorphic transformations using a composite sensor array of Raman, NIR, and ATR-UV/vis spectroscopy, FBRM, and PVM for an intelligent decision support system. *Org. Process Res. Dev.* **2015**, *19*, 167−177.
(33) Tyson, B.; Pask, C. M.; George, N.; Simone, E. Crystallization Behavior and Crystallographic Properties of dl-Arabinose and dl-Xylose Diastereomer Sugars. *Cryst. Growth Des.* **2022**, *22*, 1371−1383.

https://doi.org/10.1021/acs.iecr.2c03494
Ind. Eng. Chem. Res. 2022, 61, 18514−18529